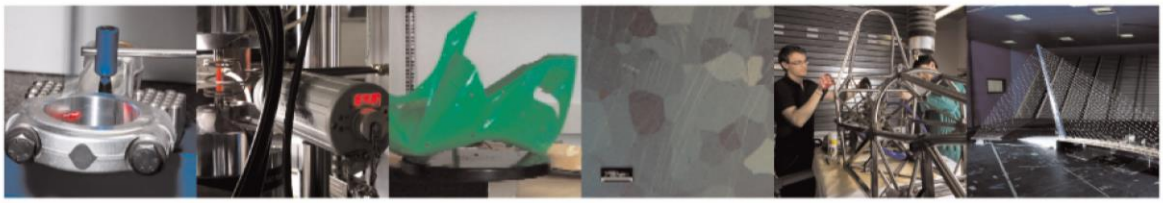

Powder bed irregularity and hot-spot detection in electron beam melting by means of in-situ video imaging

Marco Grasso, Giorgio Valsecchi, Bianca Maria Colosimo

This is a post-peer-review, pre-copyedit version of an article published in Manufacturing letters.
The final authenticated version is available online at:
http://dx.doi.org/10.1016/j.mfglet.2020.03.011

DIPARTIMENTO DI MECCANICA ■ POLITECNICO DI MILANO
via G. La Masa, 1 ■ 20156 Milano ■ EMAIL (PEC): pecmecc@cert.polimi.it
http://www.mecc.polimi.it
Rev. 0

Powder bed irregularity and hot-spot detection in Electron Beam Melting by means of in-situ video imaging

Marco Grasso[1], Giorgio Valsecchi, Bianca Maria Colosimo

Dipartimento di Meccanica, Politecnico di Milano
Via La Masa 1, 20156 Milan, Italy

[1]Corresponding author: marcoluigi.grasso@polimi.it

Abstract. The electron beam melting process has been successfully applied in various sectors to produce high-value-added products. Being a hot process operating in vacuum environment with x-rays and material vaporization among by-products, in-situ sensing and monitoring presents more challenges than in laser powder bed fusion. However, an automated and robust detection of unstable process conditions represents a key capability to meet challenging qualification requirements imposed by industry. This study presents novel in-situ monitoring methods based on high spatial resolution imaging for powder bed homogeneity monitoring and high temporal resolution video-imaging for hot-spot detection, i.e., the detection of anomalous local heat accumulations.

Keywords: electron beam melting; in-situ sensing; in-situ monitoring; powder bed; hot-spot.

1. Introduction

The electron beam melting (EBM) technology has been adopted in the recent years in the aerospace and biomedical sectors to produce high-value-added products, but its industrial development has been growing in other fields too [1 - 2]. EBM allows overcoming some common limitations of traditional manufacturing processes, but it also provides enhanced capabilities with respect to other additive manufacturing processes, e.g., high preheating temperature and high productivity. However, various defects may occur while the part is being produced and this pushes the need for the development of automated in-situ monitoring methodologies [3 – 5]. The literature on in-situ monitoring methods applied to EBM focused

on two major streams. One involves the use of infrared or near-infrared imaging either to detect volumetric flows and geometrical distortions or to predict the microstructural properties of the part [6 – 11]. The second regards the use of back-scattered electron detectors for electronic imaging. In this case, the aim consists of identifying surface pores and in-plane or out-of-plane geometrical distortions with a less expensive and more integrated sensing setup [12 – 14]. Some authors also investigated the use of embedded sensor signals to detect unstable process conditions [15 – 17].

Despite continuous developments, the in-situ monitoring capabilities in EBM are still more limited than in laser powder bed fusion (LPBF), and there is a lack of methods to automatically detect defects based on in-situ gathered data. The innovative contribution of this study consists of presenting two novel in-situ monitoring methods to address two open issues in EBM that have not been tackled in the literature so far, namely the identification of powder bed inhomogeneities and the automated detection of hot-spots, i.e., areas affected by anomalous heat accumulation. To this aim, the paper presents a sensing setup that can be easily implemented in industrial EBM systems. It involves either high spatial or high temporal resolution cameras exploiting a viewport on the top of the chamber.

Section 2 briefly describes the sensing setup; Section 3 and Section 4 respectively present the two proposed in-situ monitoring solutions. Section 5 concludes the paper and presents possible future developments.

2. Sensing setup

The proposed sensing setup relies on the viewport that is available on the top of the build chamber in Arcam EBM systems (Fig. 1). Fig. 1a shows the custom camera mounting device that was developed to enable the installation of different cameras on an Arcam A2 system. A 45 mm width Kapton® Type 100 HN rolling film was used to keep the camera lens free from metallization contamination, whereas a $60 \times 60 \times 5.5$ mm lead glass was used to shield the x-ray emissions. In this study, two cameras were installed: a high spatial resolution camera that takes pictures of the powder bed after the powder recoating, and a high temporal resolution camera that acquires high-speed videos during the melting phase. The video-image acquisition settings used in this study are shown in Fig. 1b. Both cameras work in the visible range, but they can be equipped with near infrared filters to reduce the spectrum bandwidth and the dynamic range. The field-of-view for both the cameras covers up to 90% of the build area, but

it can be further increased by modifying the aperture on the top of the heat shield. The current sensing setup enables the use of one camera at a time, but future developments may involve the use of a beam splitter to allow a multi-sensor configuration.

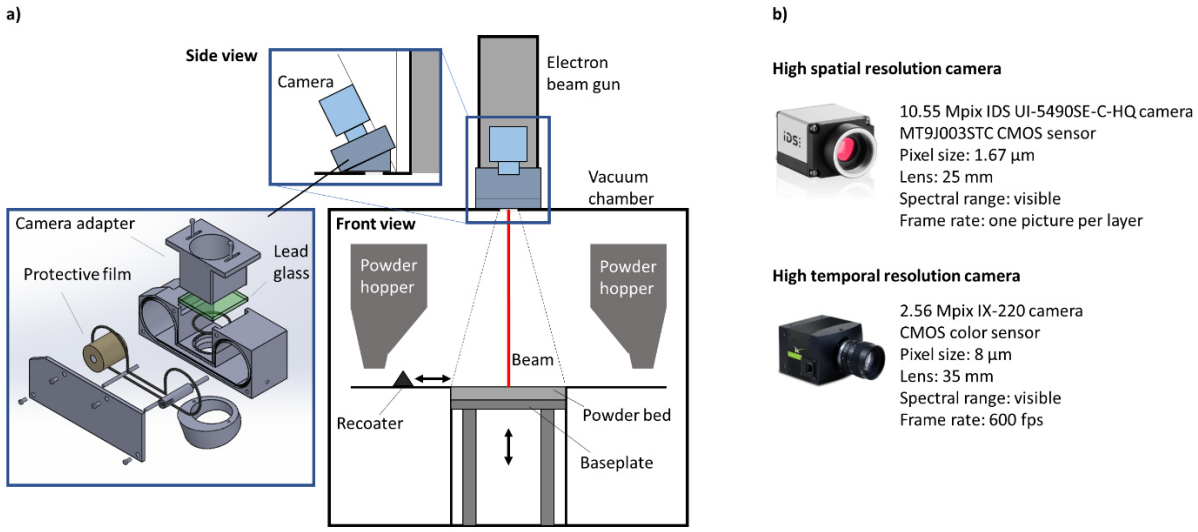

Fig. 1 – a) customized camera mounting device with rolling protective film; b) main specifications and video-imaging settings for the two cameras

3. Powder bed homogeneity monitoring

The proposed approach consists of acquiring one image after each powder recoating and signaling an alarm in the presence of powder bed irregularities. The image acquisition is triggered by the recoater current signal transition from motion to idle state. Fig. 2a shows an example of a post-recoating image after camera perspective correction where a local discontinuity in the powder bed was caused by a damage of the recoater. The brighter regions correspond to areas that were scanned by the electron beam and locally pre-/post-heated, which are hotter than the surrounding powder. An irregularity like the one shown in Fig. 2a yields a local variation of the powder bed thickness, which might cause either a swelling or volumetric defect in the part. In LPBF, the identification of this kind of inhomogeneity is made easier by the uniform pixel intensity pattern of the powder bed [18 – 20]. In EBM, the presence of areas with different brightness caused by different cooling gradients imposes the use of additional image pre-processing operations. The proposed methodology envisages two pre-processing steps. First, a background subtraction based on the concept of the 'rolling ball' algorithm [21] is used to smooth the background pixel intensities, followed by a thresholding operation [22] to isolate darker areas (Fig. 2b). The second step consists of a morphological erosion operation

to remove isolated pixels and small connected components caused by image noise. The connected components obtained at the end (Fig. 2c) are representative of irregularities in the powder bed. More details about the image processing methodology and a comparison against alternative image segmentation methods are discussed in the Supplementary Material.

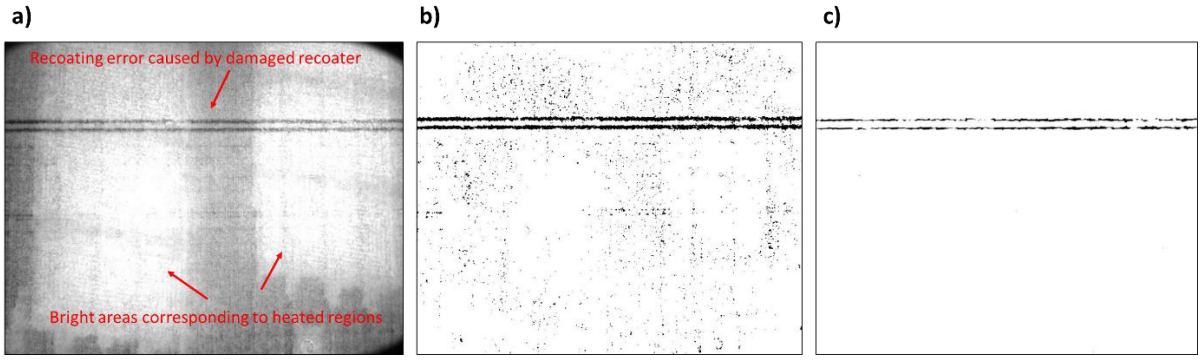

Fig. 2 – a) original post-recoating image, b) image after background subtraction and thresholding operation, c) final defect identification after morphological operations

An alarm rule based on the area of the identified connected components can be designed to automatically signal the presence of a non-homogeneous powder recoating. Irregularities in the powder bed may introduce undesired variability and discontinuities in the properties of the material. The proposed approach enables their automated detection and it is easy to implement in EBM systems. Future experimentations will be aimed at characterizing its performances and robustness. A further future development consists of combining the layerwise image acquisition with an illumination source to further enhance the quality of the image.

4. Hot-spot detection

A hot-spot consists of a local over-heating of the layer caused by a diminished heat flow towards the surrounding material [23 – 24]. The region of the part where the hot-spot occurs is affected by an anomalous heat accumulation and a slower cooling transitory. Hot-spots may change the solidification mechanism of the material leading to geometrical distortions and microstructural discontinuities, both in EBM and LPBF, but local overheating may also cause an increase of material vaporization in EBM [25]. Hot-spots and powder bed irregularities can be causally related [23 – 24]: on the one hand, an out-of-plane distortion caused by local heat

accumulation may damage the recoater and, on the other hand, a local decrease of powder bed thickness may increase the local energy density and produce a hot-spot event.

Previous studies in LPBF [23 – 24] showed that a spatio-temporal Principal Component Analysis (ST-PCA) methodology was suitable to separate the hot-spot from the natural process dynamic in LPBF. The hot-spot generating mechanism is analogous in EBM and LPBF. However, in L-PBF, the presence of plume and spatters makes the pixel intensity patterns more "wild" than in EBM, as shown in [23] and [24]. This motivates the proposal of a simplified alarm rule in our study with respect to the one investigated in L-PBF, which makes the overall algorithm also much more computationally efficient. The proposed method relies on the fact that the pixel intensity time series in the presence of a hot-spot exhibits a high intensity for a certain time interval followed by a slow cooling transitory as shown in Fig. 3.

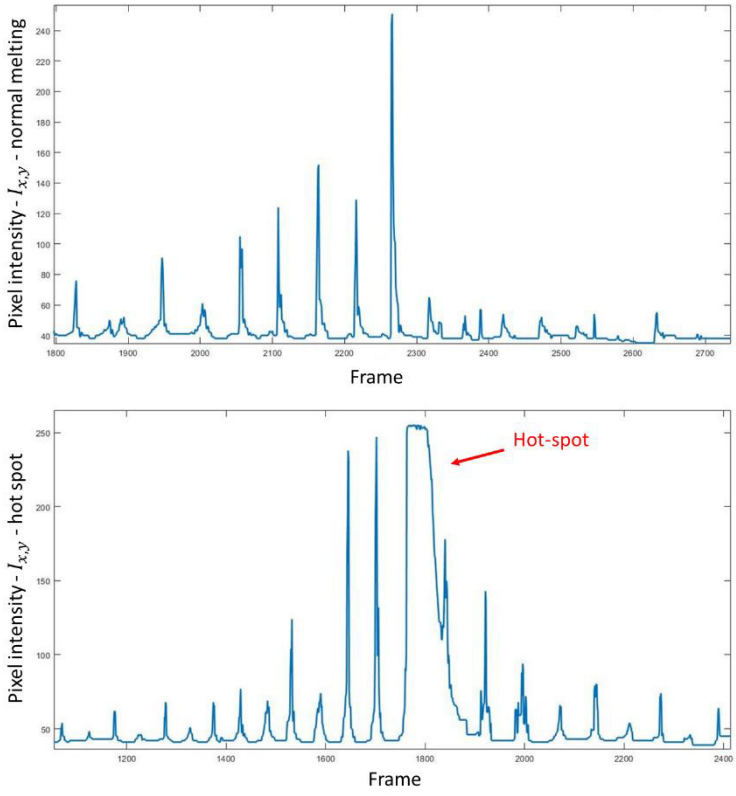

Fig. 3 – Comparison between a pixel intensity time series during the EBM with in-control process behavior (top panel) and in the presence of a hot-spot (bottom panel)

A synthetic index was computed as $S_I(x,y) = \sum_{t=0}^{T} \mathcal{I}(I_t(x,y) > k_1 \;\&\; \Delta I(x,y) < k_2)$, where $\mathcal{I}(\cdot)$ is the indicator function, $I_t(x,y)$ is the pixel intensity of the (x,y)-th pixel in the t-th frame, $\Delta I(x,y)$ is the difference of (x,y)-th pixel intensities in the t-th and $(t-1)$-th frames

and k_1 and k_2 are constants to be defined during a calibration phase. The estimate of $S_I(x, y)$ can be iteratively updated as new video frames are acquired.

Fig. 4a shows the 2D map of $S_I(x, y)$ estimated during the EBM of a lattice component (diameter 40 mm) where some local hot-spots were observed, possibly caused by irregularities in the power bed. Fig. 4b compares the proposed descriptor with the T^2 synthetic index proposed in [24]. Both the descriptors identified the hot-spot region, but the proposed approach is two orders of magnitude more computationally efficient than the competitor. This comes at the expense of the need to define two additional thresholds, respectively on the pixel intensity and its derivative. The Supplementary Material presents some guidelines on the choice of k_1 and k_2, together with the results of a sensitivity analysis with respect to these two parameters. To the aim of automated hot-spot detection, the same clustering-based alarm rule presented in [24] can be applied to the descriptor proposed in this study.

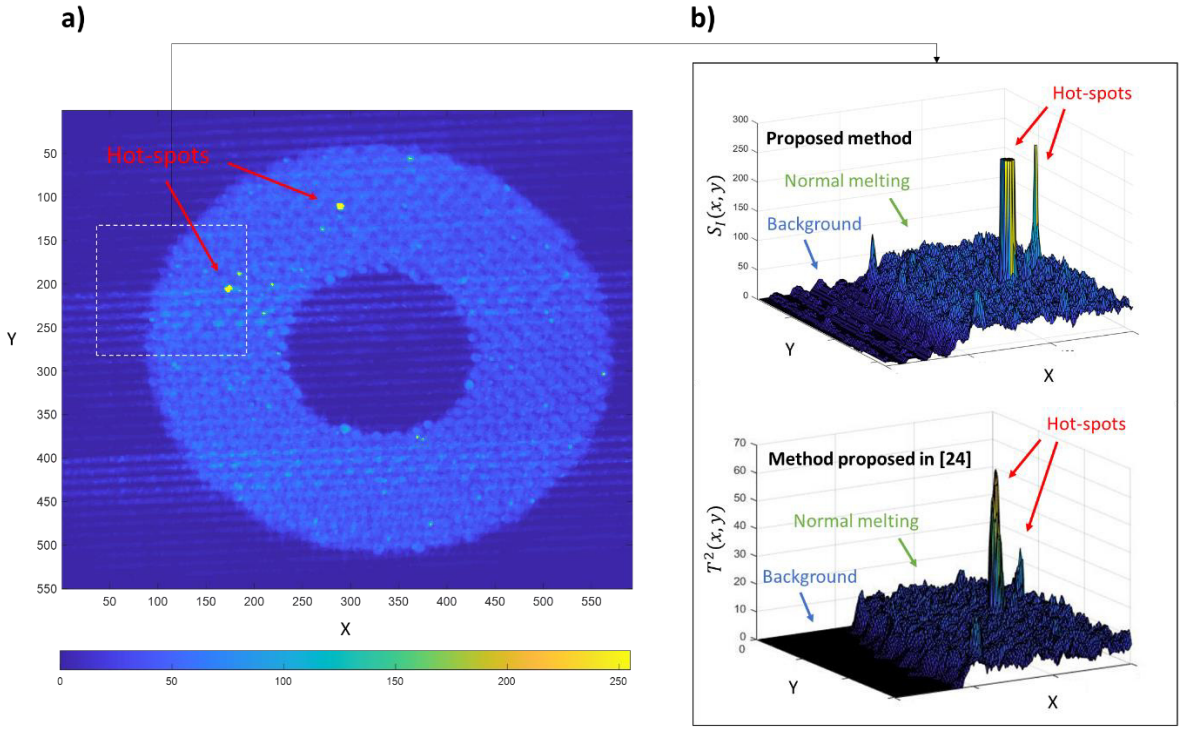

Fig. 4 – a) 2D map of the $S_I(x, y)$ descriptor proposed for automated hot-spot detection; b) comparison between our proposed descriptor and the one proposed in [24], where k_1 and k_2 were set at 90% and 10% of the maximum pixel intensity, respectively

5. Conclusions

This study presented two novel in-situ monitoring methods suitable to detect either local irregularities in the powder bed or local heat accumulations in the printed slice. The two methods provide complementary information that can be used to quickly identify departures from a stable and in-control EBM process. Their feasibility was discussed by means of real examples based on experimental activities on an Arcam A2 system. Future developments will focus on the characterization of the in-situ monitoring performances in terms of false alarms and actual defect detection capability, on the feasibility analysis of real-time implementation and on the evaluation of the correlation between in-situ detected anomalies and actual defects in the produced part.

References

[1] Körner, C. (2016). Additive manufacturing of metallic components by selective electron beam melting—a review. International Materials Reviews, 61(5), 361-377.

[2] Zhang, L. C., Liu, Y., Li, S., & Hao, Y. (2018). Additive manufacturing of titanium alloys by electron beam melting: A review. Advanced Engineering Materials, 20(5), 1700842.

[3] Grasso, M., & Colosimo, B. M. (2017). Process defects and in situ monitoring methods in metal powder bed fusion: a review. Measurement Science and Technology, 28(4), 044005.

[4] Everton, S. K., Hirsch, M., Stravroulakis, P., Leach, R. K., & Clare, A. T. (2016). Review of in-situ process monitoring and in-situ metrology for metal additive manufacturing. Materials & Design, 95, 431-445.

[5] Mani, M., Feng, S., Lane, B., Donmez, A., Moylan, S., & Fesperman, R. (2015). Measurement science needs for real-time control of additive manufacturing powder bed fusion processes, NISTIR Report 8036, http://dx.doi.org/10.6028/NIST.IR.8036

[6] Raplee, J., Plotkowski, A., Kirka, M. M., Dinwiddie, R., Okello, A., Dehoff, R. R., & Babu, S. S. (2017). Thermographic microstructure monitoring in Electron Beam Additive Manufacturing. Scientific reports, 7, 43554.

[7] Dehoff, R.R., (2019). Electron beam melting technology improvements, Crada Final Report NFE-12-04045, January 18, 2019

[8] Nandwana, P., Kirka, M. M., Paquit, V. C., Yoder, S., & Dehoff, R. R. (2018). Correlations Between Powder Feedstock Quality, In Situ Porosity Detection, and Fatigue

Behavior of Ti-6Al-4V Fabricated by Powder Bed Electron Beam Melting: A Step Towards Qualification. JOM, 70(9), 1686-1691.

[9] Cordero, P. M., Mireles, J., Ridwan, S., & Wicker, R. B. (2017). Evaluation of monitoring methods for electron beam melting powder bed fusion additive manufacturing technology. Progress in Additive Manufacturing, 2(1-2), 1-10.

[10] Rodriguez, E., Mireles, J., Terrazas, C. A., Espalin, D., Perez, M. A., & Wicker, R. B. (2015). Approximation of absolute surface temperature measurements of powder bed fusion additive manufacturing technology using in situ infrared thermography. Additive Manufacturing, 5, 31-39.

[11] Boone, N., Zhu, C., Smith, C., Todd, I., & Willmott, J. R. (2018). Thermal near infrared monitoring system for electron beam melting with emissivity tracking. Additive Manufacturing, 22, 601-605.

[12] Pobel, C. R., Arnold, C., Osmanlic, F., Fu, Z., & Körner, C. (2019). Immediate development of processing windows for selective electron beam melting using layerwise monitoring via backscattered electron detection. Materials Letters, 249, 70-72.

[13] Wong, H., Neary, D., Jones, E., Fox, P., & Sutcliffe, C. (2019). Pilot feedback electronic imaging at elevated temperatures and its potential for in-process electron beam melting monitoring. Additive Manufacturing, 27, 185-198.

[14] Wong, H., Neary, D., Jones, E., Fox, P., & Sutcliffe, C. (2019). Benchmarking spatial resolution in electronic imaging for potential in-situ Electron Beam Melting monitoring. Additive Manufacturing, 29, 100829.

[15] Yoder, S., Nandwana, P., Paquit, V., Kirka, M., Scopel, A., Dehoff, R. R., & Babu, S. S. (2019). Approach to qualification using E-PBF in-situ process monitoring in Ti-6Al-4V. Additive Manufacturing, 28, 98-106.

[16] Grasso M., Gallina F., Colosimo B.M. (2018), Data Fusion Methods for Statistical Process Monitoring and Quality Characterization in Metal Additive Manufacturing, 15th CIRP Conference on Computer Aided Tolerancing – CIRP CAT 2018, June 2018, Milan, Italy

[17] Steed, C. A., Halsey, W., Dehoff, R., Yoder, S. L., Paquit, V., & Powers, S. (2017). Falcon: Visual analysis of large, irregularly sampled, and multivariate time series data in additive manufacturing. Computers & Graphics, 63, 50-64.

[18] Foster, B., Reutzel, E., Nassar, A., Hall, B., Brown, S., & Dickman, C. (2015, August). Optical, layerwise monitoring of powder bed fusion. In Solid Freeform Fabrication Symposium, Austin, TX, Aug (pp. 10-12).

[19] Caltanissetta F., Grasso M., Petrò S., Colosimo, B. M. (2018). Characterization of In-Situ Measurements based on Layerwise Imaging in Laser Powder Bed Fusion, Additive Manufacturing, 24, 183-199

[20] Zur Jacobsmühlen, J., Kleszczynski, S., Witt, G., & Merhof, D. (2015). Elevated region area measurement for quantitative analysis of laser beam melting process stability. In 26th International Solid Freeform Fabrication Symposium; Austin, TX (pp. 549-559).

[21] Sonka, M., Hlavac, V., & Boyle, R. (2014). Image processing, analysis, and machine vision. Cengage Learning, Fourth Edition.

[22] El-Zaart, A. (2010). Images thresholding using ISODATA technique with gamma distribution. Pattern Recognition and Image Analysis, 20(1), 29-41.

[23] Grasso M., Laguzza V., Semeraro Q., Colosimo B.M., (2017), In-process Monitoring of Selective Laser Melting: Spatial Detection of Defects via Image Data Analysis, Journal of Manufacturing Science and Engineering, 139(5), 051001-1 - 051001-16.

[24] Colosimo, B.M., Grasso, M. (2018), Spatially weighted PCA for monitoring video image data with application to additive manufacturing, Journal of Quality Technology, 50(4), 391-417

[25] Schwerdtfeger, J., Korner, C. (2014). Selective electron beam melting of Ti-48Al-2Nb-2Cr: Microstructure and aluminium loss, Intermetallics, 49, 29-35

Supplementary Material

6. Introduction

This document includes additional material for the paper "Powder bed irregularity and hot-spot detection in Electron Beam Melting by means of in-situ video imaging".

Section 2 presents a comparison analysis between the proposed approach for powder bed image processing and alternative algorithms. Section 3 presents some practical guidelines for the choice of k_1 and k_2 in the proposed approach for in-line hot-spot detection and a sensitivity analysis with respect to these two parameters.

7. Powder bed homogeneity monitoring

The image processing method for powder bed irregularity detection consists of three operations, which are detailed hereafter. The results presented here refer to the same image used as an example in the paper. The overall test dataset consists of 50 images of a defective powder bed caused by a damage of the recoater.

Step 1 - background subtraction

The background of the layerwise image acquired after the powder recoating is characterized by bright areas within and around the previously scanned slices, where the temperature is higher than the surrounding powder. The goal of the background subtraction operation consists of smoothing the pixel intensity variations to reduce the background contrast caused by the presence of hot and cold regions in the powder bed. The 'rolling ball' algorithm [1] is a method commonly used to this aim. It involves a controllable parameter, i.e., the rolling ball radius, r, which is related to the size of the foreground features that should not be filtered out. The smaller the radius, the smaller the features of the image that will be smoothed and filtered out. The higher the radius, the lower is the background attenuation. Fig. 1 shows one original powder bed image during the EBM process and examples of background subtraction results with different values of r. With $r = 1$ pixel, both salient background and foreground features are filtered out, whereas, with $r = 50$ pixels, the contrast in the powder bed areas is quite high. In

this study, a rolling ball radius $r = 10$ pixels was used as a compromise choice, but a further tuning of this parameter will be investigated in a future study.

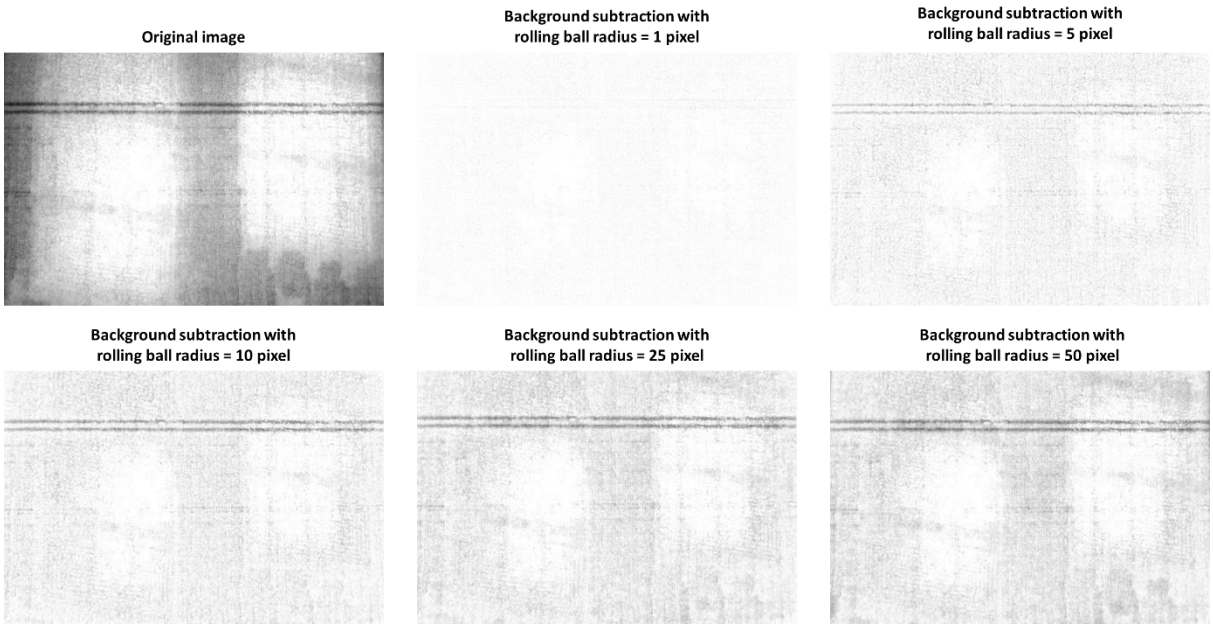

Fig. 1 – Original image and examples of background subtraction results with different choices of the rolling ball radius

Step 2 – Thresholding

The thresholding operation is aimed at isolating darker areas corresponding to the irregularities in the powder recoating. Fig. 2 shows a comparison of different common thresholding methods [2] applied to the image in Fig 1 after background subtraction with $r = 10$. The method proposed in this study is based on the IsoData algorithm [3], which involves an iterative identification of the threshold by comparing the average intensity in the background and foreground regions. Fig. 2 shows that the proposed approach and the Otsu's method [4] yield similar results, whereas other methods, i.e., the so-called "moments" algorithm [5] and the Huang's algorithm [6], are more affected by the noise of pixel intensity in the background region, which may produce worst results in the detection of the actual irregularities of interest.

The threshold is estimated on a layer-by-layer basis, relying on the histogram properties of the powder bed image after the background subtraction.

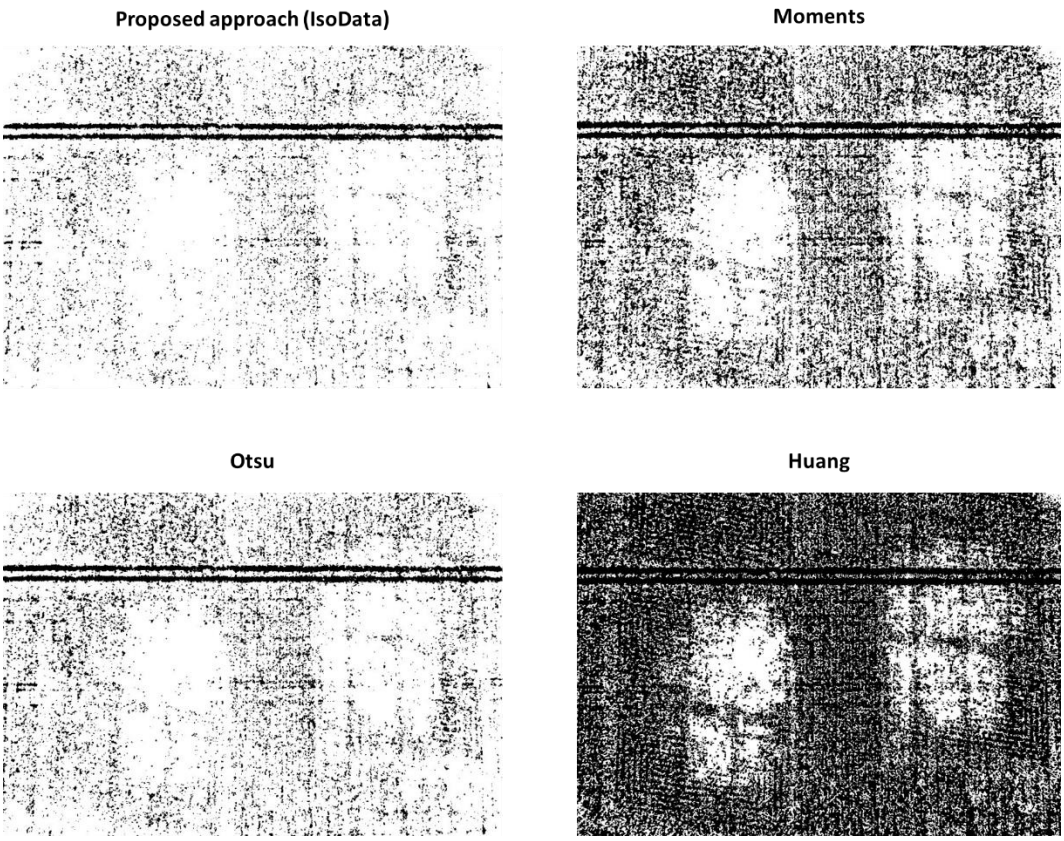

Fig. 2 – Comparison of four different thresholding methods applied to one powder bed image after background subtraction with $r = 10$

Step 3 – Morphological operation

The last step consists of a simple erosion operation [1] applied to the connected components identified in the image after image thresholding. This operation removes the two most external pixels from the edges of each connected component in the binary image. This operation resulted sufficient to get rid of more than 98.5% of small connected components caused by noise and artefacts in the background in all tested images.

After the erosion operation, a clear isolation of the region of interest corresponding to the defect in the powder bed is obtained. Future developments will be devoted to design an automated alarm rule to signal the occurrence of an irregular powder recoating and to characterize the effect of such irregularity on the final quality of the produced parts.

Moreover, a more extended experimental study is needed to characterize the actual performances of the proposed image processing method. This further analysis will also allow

tuning the overall methodology with respect to different conditions that may arise during the production of complex parts via EBM.

8. Hot-spot detection

The proposed approach for hot-spot detection requires setting two threshold values, i.e., k_1 and k_2. Table 1 shows the results of a sensitivity analysis of hot-spot detection performances with respect to the values of these two parameters. This analysis was based on one layer monitored during the production of complex shapes where different hot-spot events occurred in a lattice component. The pixels where the hot-spot events occurred were manually labelled and the proposed approach was tested with different choices of k_1 and k_2 in the following ranges: $k_1 \in [0.5 - 1] \cdot I_{max}$ and $k_1 \in [0.1 - 0.5] \cdot I_{max}$, where I_{max} is the maximum intensity in the video-image data. Assuming that the image histogram covers the entire range of pixel intensity values, $I_{max} = 255$ for 8-bit images. This saturation intensity is achieved in the melt pool and heat affected zones. The metrics used to determine the hot-spot detection performances in Table 1 are the percentage of pixels belonging to hot-spot regions properly detected as hot-spots and the percentage of pixels in the scanned area wrongly signalled as hot-spots (false alarms).

Table 1 – Sensitivity analysis of the hot-spot detection method with respect to k_1 and k_2.

Threshold parameters		Hot-spot detection	False alarms
k_1	k_2		
$0.5 \cdot I_{max}$	$0.1 \cdot I_{max}$	100%	0%
	$0.25 \cdot I_{max}$	100%	0%
	$0.5 \cdot I_{max}$	100%	0.05%
$0.7 \cdot I_{max}$	$0.1 \cdot I_{max}$	100%	0%
	$0.25 \cdot I_{max}$	100%	0%
	$0.5 \cdot I_{max}$	100%	0.01%
$0.9 \cdot I_{max}$	$0.1 \cdot I_{max}$	100%	0%
	$0.25 \cdot I_{max}$	100%	0%
	$0.5 \cdot I_{max}$	100%	0%
I_{max}	$0.1 \cdot I_{max}$	65%	0%
	$0.25 \cdot I_{max}$	65%	0%
	$0.5 \cdot I_{max}$	35%	0%

Table 1 shows that the hot-spots were properly detected with $0.5 \cdot I_{max} \leq k_1 < I_{max}$ and $k_2 < 0.5 \cdot I_{max}$. When $k_1 = I_{max}$ the hot-spot detection capability decreases as the threshold value is too high. Indeed, the maximum intensity in the hot-spot areas was slightly lower than the saturation point for most of the frames. On the other hand, when $k_2 \geq 0.5 \cdot I_{max}$, the threshold on the variation of the intensity becomes not fully effective in isolating pixels whose intensity remains stable for a certain period of time. In this case, a too high threshold results in a higher probability of false alarms. With our camera settings, the pixel intensity drop during the normal cooling phase is larger than 200, i.e., about $0.8 \cdot I_{max}$. Therefore, the closer is the value of k_2 to this drop, the higher is the risk to signal false alarms.

Based on these results, the following guidelines can be followed to set the values of parameters k_1 and k_2 in the proposed hot-spot detection methodology. The value of k_1 can be set at an intensity close to the saturation point, e.g., at about 80 - 90% of the pixel saturation intensity, I_{max}. The value of parameter k_2 can be set at a small percentage of the pixel saturation intensity, e.g. 10 – 20%.

References

[1] Sonka, M., Hlavac, V., & Boyle, R. (2014). Image processing, analysis, and machine vision. Cengage Learning, Fourth Edition.

[2] Gonzales-Barron, U., & Butler, F. (2006). A comparison of seven thresholding techniques with the k-means clustering algorithm for measurement of bread-crumb features by digital image analysis. Journal of food engineering, 74(2), 268-278.

[3] El-Zaart, A. (2010). Images thresholding using ISODATA technique with gamma distribution. Pattern Recognition and Image Analysis, 20(1), 29-41.

[4] Otsu, N. (1979), A threshold selection method from gray-level histograms, IEEE Transactions on Systems, Man and Cybernetics, 9:62-66

[5] Tsai, W. (1985), Moment-preserving thresholding: a new approach, Computer Vision, Graphics, and Image Processing, 29: 377-393

[6] Huang, L-K. & Wang, M-J. J. (1995), Image thresholding by minimizing the measure of fuzziness, Pattern Recognition, 28(1): 41-51